Tea-polyphenols coatings on AZ31 and AZ91 magnesium alloys for degradation control and improvement of the biological response

Applied Surface Science 721 (2026) 165402

Contents lists available at ScienceDirect

Applied Surface Science

journal homepage: www.elsevier.com/locate/apsusc

Full Length Article

Tea-polyphenols coatings on AZ31 and AZ91 magnesium alloys for degradation control and improvement of the biological response

S. Ferraris [a,*], S. Spriano [a], F. Gamna [a], M. Saqib [b], N. Beshchasna [b], J. Opitz [b], A.R. Boccaccini [c], Irem Unalan [c], K. Naplocha [d], A. Dmitruk [d]

[a] Politecnico di Torino, Department of Applied Science and Technology, Turin, Italy
[b] Fraunhofer Institute for Ceramic Technologies and Systems IKTS, Dresden, Germany
[c] Department of Materials Science and Engineering, University of Erlangen-Nuremberg, Erlangen, Germany
[d] Department of Lightweight Elements Engineering, Foundry and Automation, Faculty of Mechanical Engineering, Wroclaw University of Science and Technology, Wroclaw, Poland

ARTICLE INFO

Keywords:
Mg-alloys
Degradation
Polyphenols
Coating

ABSTRACT

Magnesium alloys are promising materials for biodegradable orthopedic and cardiovascular implants, avoiding second interventions and related complications. Magnesium is a biocompatible and key element for numerous physiological processes; however, its degradation rate is too rapid, accompanied by strong hydrogen development, pH rise, and consequent inflammation.

In this context, innovative strategies to modulate the degradation of magnesium and its alloys are an urgent clinical need.

Natural green tea polyphenols were explored in this research work as a promising and sustainable strategy for obtaining organic protective coatings on AZ31 and AZ91 Mg-alloys for cardiovascular and orthopedic applications. Coatings were obtained by soaking samples in a water-based polyphenolic solution and characterized by Scanning Electron Microscopy equipped with Energy Dispersive Spectroscopy, Fourier Transformed Infrared Spectroscopy, tape adhesion tests, static soaking degradation tests, electrochemical corrosion measurements, and preliminary cytocompatibility tests.

Results suggest that surface preparation plays a crucial role in obtaining stable and homogeneous coatings. In optimized conditions, globular-shaped coatings free of cracks were obtained on both alloys. These coatings significantly reduced the corrosion rate in electrochemical tests and had a protective effect on cells.

1. Introduction

Trauma and Coronary Artery Diseases (CAD) are among the most widespread and diffused pathologies which require medical treatments worldwide [1–3]. The high medical costs of these treatments (about 30–50 billion dollars per year for bone implants [1,2]) are significantly increased if surgical removal of implants is required after bone healing. Moreover, complications and reintervention are critical for patient health [1–3]. Bioresorbable vascular devices are essential in coronary artery disease as they provide temporary support to the vessel while gradually dissolving, allowing natural healing and restoring normal vascular function without leaving a permanent implant.

The possibility of treating cardiovascular and orthopedic diseases with fully resorbable temporary metallic implants has sparked the interest of scientists and surgeons since the end of the 19th century, posing magnesium-based biomaterials as a groundbreaking alternative to traditional highly corrosion-resistant implantable metals [4].

Magnesium is a biocompatible and essential nutrient in the human body with key functions in metabolic processes (e.g. synthesis of proteins, enzyme activation, neuromuscular and heart functions regulation). Moreover, it has an elastic modulus (40–45 GPa) and density (1.73 g/cm^3) close to cortical bone (5–23 GPa and 1.6–2 g/cm^3, respectively), and it is completely biodegradable [5,6].

These features make magnesium and its alloys promising materials for bioresorbable temporary orthopedic and cardiovascular implants, as demonstrated by numerous research studies and some clinical applications [1,2,7].

However, a fast and not completely controllable degradation rate,

* Corresponding author.
E-mail address: sara.ferraris@polito.it (S. Ferraris).

https://doi.org/10.1016/j.apsusc.2025.165402
Received 20 August 2025; Received in revised form 26 November 2025; Accepted 26 November 2025
Available online 29 November 2025

imbalance between degradation and tissue regeneration, hydrogen development, local pH rise, and consequent inflammation reaction still represent significant obstacles to the development and widespread clinical application of Mg-based materials [1,2,7].

Several solutions are currently under investigation to modulate and control the degradation rate and relative issues, making the successful and widespread application of biodegradable Mg-based alloys possible in the context of implants. Strategies explored in the scientific literature range from the design of the alloy composition, to surface modifications (e.g. plasma, ion implantation, laser) or barrier coatings (e.g. calcium phosphates, metal oxides and hydroxides, MgF_2, polymers) obtained by various techniques such as Plasma electrolytic oxidation (PEO), hydrothermal synthesis, electrodeposition, spin/dip coating, Layer by Layer, electrostatic spraying, and sol–gel to cite some examples [8–14].

To further enhance barrier properties of widely investigated PEO coatings, several protective top layers have been reported in the literature in combination with the inorganic porous layer: the combination of albumin and magnesium sulphate [15], hydroxyapatite nanoparticles [16], layered double hydroxide (LDH) and metal–organic frameworks (MOFs) [17] or a bioresorbable polymer (polycaprolactone, PCL) with halloysite nanotubes (HNTs) loaded with a corrosion inhibitor (benzotriazole, BTA) [18].

Recently, polyphenols-based protective coatings on Mg-based alloys for biomedical applications have been gaining increasing interest [19–25] due to the corrosion protection ability of polyphenols coupled with their anti-inflammatory, antibacterial, antioxidant, osteogenic, and vasculoprotective properties.

In the present research, green tea polyphenols were used for homogeneous protective coatings on AZ31 and AZ91 magnesium alloys, with a focus on the cardiovascular and orthopedic fields, respectively. Physical and chemical characterizations (Scanning Electron Microscopy equipped with Energy Dispersive Spectroscopy – SEM-EDS, Fourier Transformed Infrared Spectroscopy in Attenuated Total Reflectance – FTIR-ATR, tape adhesion test) were performed. The morphology, chemical composition, and adhesion to the substrates of the coating are reported. Corrosion resistance was evaluated both by static immersion in phosphate buffer solution (PBS) and by means of electrochemical tests, evidencing a strong dependence of the results on the testing conditions. Finally, preliminary biological characterizations were performed by using normal human dermal fibroblast cells (NHDF) in order to evaluate the protection ability of tea polyphenols coating on cells from the adverse effects of Mg-alloys degradation.

2. Materials and methods

2.1. Samples preparation

AZ31 Mg alloy was purchased from Goodfellow in the form of plane sheets 1 mm thick and cut into square samples (1x1 cm) by means of shears. Samples were used as cut or after polishing with SiC abrasive papers up to 4000 grit on both sides (see Table 1 for the samples' acronyms). A polished and regular surface is in line with cardiovascular applications, which are typical for this alloy.

Table 1
Samples preparation conditions and acronyms.

Acronym	Description
TPH	Green tea polyphenols
AZ31	AZ31 as-received and washed
AZ31-pol	AZ31 polished and washed
AZ31-TPH30	AZ31 polished, washed, and coated with tea polyphenols at 30 mg/ml, 10 min in orbital shaker
AZ91	AZ91 as-cast and washed
AZ91-blast	AZ91 blasted and washed
AZ91-TPH30	AZ91 blasted, washed, and coated with tea polyphenols at 30 mg/ml, 10 min in orbital shaker

AZ91 samples were cast at the Wroclaw University of Science and Technology, as previously described by the authors [24,25], by the combination of 3D printing and investment casting. Samples were considered as prepared or after blasting. Sand-blasting of the samples' surface was performed by spraying the abrasive at an angle of 45° until the sample was visibly cleaned (see Table 1 for the samples' acronyms). A rough surface is well-suited for cone contact applications, which are typical of this alloy.

All samples were washed in ethanol for 5 min in an ultrasonic bath, rinsed in ultrapure water and dried with compressed air before polyphenols coating.

2.2. Polyphenols coating

Polyphenols were extracted from green tea leaves (Longjing, Hangzhou, China) by conventional solvent extraction in an ethanol–water mixture at 60 °C as previously reported by the authors [26] and referred to as TPH from now on. Freeze dried polyphenols were used for the preparation of functionalization solutions, then used at 37 °C, as described in the following, in order to facilitate grafting without degradation of the active molecules.

Polyphenol solutions were prepared by dissolving freeze-dried extract in ultrapure water at different concentrations (5, 10, 20, 30, 50 mg/ml), the pH of polyphenols solutions ranges from 5.4 to 4.8 (from lower to higher concentrations).

Mg-alloy samples were soaked in polyphenols solutions at 37 °C in static (multi-well plate in incubator) or dynamic (orbital shaker, 120 rpm) conditions for different times (from 10 min to 45 min).

At the end of soaking, samples were washed in ultrapure water or sonicated in ethanol for 5 min and subsequently washed in ultrapure water and finally dried in the incubator at 37 °C.

Table 1 summarizes the acronyms and preparation conditions of samples selected for the characterization described in the present paper. Experimental conditions excluded from preliminary characterizations will be only cited for comparison in the discussion of the results and in the Supplementary Material.

2.3. Surface characterizations

Surface topography, before and after coating, as well as surface chemical composition were investigated by means of Scanning Electron Microscopy equipped with Energy Dispersive Spectroscopy (SEM, JEOL, JCM 6000 plus, EDS, JEOL, and JED 2300) setting the voltage at 15 kV.

A further insight into the surface chemical composition was obtained by means of Fourier Transformed Infrared Spectroscopy in Attenuated Total Reflectance mode (FTIR-ATR, Nicolet iS50 FTIR Spectrometer, Thermo Scientific, Waltham, MA, USA), both for green tea extracts and on Mg alloy samples before and after coating. Background was recorded in air before each measurement set and subtracted by the instrument software (OMNIC).

Coating adhesion was estimated by means of the cross-cut tape adhesion test according to the ASTM D3359 standard [27]. Briefly a grid of parallel cuts was obtained on the surface with the cutter available in the measurement kit, the tape was applied on the engraved surface and removed. The surface was finally inspected and macro-images taken. SEM images were also acquired for a better understanding of coating adhesion.

Static degradation of coated and uncoated Mg-alloy samples was investigated according to the ASTM G31-72 standard [28]. Each sample was soaked in PBS (Phosphate Buffered Saline 79382-50TAB Sigma Aldrich) considering to have a ratio between the volume of the solution (V_{sol}) and the external surface of the sample (S_s) higher than 30 ml/cm^2, as suggested by the standard. Samples were soaked for different experimental times up to 7 days and the solution was refreshed every 3 days. After immersion, samples were visually inspected and pH and Mg concentration of the soaking solution were evaluated by means of a pH

meter and a portable photometer specific for Mg and Ca ions (Calcium and Magnesium Photometer HI97752, Hanna Instruments, Woonsocket, RI, USA), respectively. Polyphenols release in PBS was estimated by means of the Folin&Ciocalteu test.

2.4. Electrochemical tests

2.4.1. The electrochemical cell

A standard three-electrode electrochemical cell was utilized for this study, with AZ31 and AZ91 surfaces (Table 1) serving as the working electrode (WE). A silver/silver chloride (Ag/AgCl) electrode functioned as the reference electrode (RE), while a platinum rod (3 mm diameter) was employed as the counter electrode (CE). Potentiodynamic measurements were conducted using the Autolab PGSTAT204 potentiostat (Metrohm, Herisau, Switzerland), with programming and data recording managed through Nova advanced electrochemical software 2.x (Metrohm, Herisau, Switzerland). Various simulated physiological solutions with different complexity have been explored to monitor the behavior of Mg-alloys. The electrolytes used in the electrochemical cell included phosphate-buffered saline (PBS; 1 tablet per 100 mL of ultrapure water), Hanks' Balanced Salt Solution with Phenol Red and without $Ca2^{+}$ and $Mg2^{+}$ (HBSS; Lonza, Vivers, Belgium), Ringer's infusion solution (Ringer; B. Braun, Hessen, Germany), HBSS without Phenol Red (HBSS2; Lonza, Vivers, Belgium), and Dulbecco's Modified Eagle's Medium (DMEM; Gibco™, Thermo Fisher Scientific, Waltham, MA, USA). Chemical composition of electrolytes used in electrochemical experiment is provided in Table 2. These solutions were selected because they are widely used as physiological electrolytes for in-vitro degradation and corrosion assessment of Mg-based alloys and represent clinically relevant ionic environments.

For each measurement, 20 mL of the respective test fluid was added to the electrochemical cell. The exposed surface area of all samples was in the range of 0.2827 cm^2. All electrochemical studies were performed at room temperature (23–25 °C).

2.4.2. Electrochemical measurements

The electrochemical measurements were conducted by first measuring the open-circuit potential (OCP), and then potentiodynamic polarization by linear sweep voltammetry (LSV), for which Tafel plots were derived in order to determine corrosion behavior. Prior to OCP measurement, the samples were immersed in the electrolyte for 15 min without any electrochemical perturbation to allow potential stabilization, following the procedure established in our previous work [29]. For each measurement, 20 mL of electrolyte (HBSS, HBSS2, DMEM, PBS, ringer) was used with specimens exposing 0.2827 cm^2 of area. A stable OCP was achieved at which point corrosion current density (I (mA/cm^2)) was recorded against WE potential (E (V) vs. Ag/AgCl). Potentiodynamic polarization curves were obtained by applying a potential sweep from −0.5 V (cathodic) to + 0.5 V (anodic) relative to the OCP for all samples, with a scan rate of 10 mV/s and 1 mV step size between data points. At least five potentiodynamic scans were carried out on each sample in each test medium. Tafel curves were obtained using log-transformed current density values against WE potential. Tafel curves were then automatically analyzed by NOVA electrochemical analysis software version 2.x (Metrohm, Herisau, Switzerland) to determine the corrosion current density (i_{corr}) and corrosion potential (E_{corr}) after manual extrapolation. Similarly, Tafel curves for each sample were reproduced for visual output and further processing by using MS Excel. Corrosion rates were calculated by the NOVA software based on ASTM G102-89 standard [30] through the formula:

$$CR = K_1 \frac{i_{corr}}{\rho} EW$$

Here, the corrosion rate (CR) is in mm/year, K_1 is 3.27 × 10^{-3} mm·g/μA·cm·yr, i_{corr} is the corrosion current density (μA/cm^2), ρ is the density of the material (g/cm^3), and EW is the equivalent weight (g/eq). EW and ρ for AZ31 are 12.3 g/eq and 1.77 g/cm^3, respectively, and those for AZ91 are 11.89 g/eq and 1.81 g/cm^3, respectively [24].

Table 2
Chemical composition of fluids used in electrochemical tests.

Composition	Concentration (g/L)				
	HBSS	HBSS2	DMEM	PBS	Ringer
NaCl	8.000	8.000	6.400	8.000	8.600
KCl	0.400	0.400	0.400	0.200	0.300
$MgSO_4$	–	0.2	0.0977	–	–
$CaCl_2$	–	0.186	0.200	–	0.330
$NaHCO_3$	0.350	0.350	3.700	–	2.200
Na_2HPO_4	0.009	0.009	–	1.44	0.130
NaH_2PO_4	–	–	0.125	–	0.030
KH_2PO_4	0.006	0.006	–	0.24	–
$C_6H_{12}O_6$ (Dextrose)	1.000	1.000	4.500	–	–
$C_{19}H_{14}O_5S$ (Phenol red)	0.002	–	–	–	–

2.4.3. Biological characterization

The cell proliferation of tea polyphenol-coated AZ31 and AZ91 magnesium alloys was assessed by a direct contact assay according to the ISO-10993–5 standard test method and previous work [31]. Briefly, human dermal fibroblast cells (NHDF) cells were seeded on top of the magnesium alloys at a density of 25 × 10^3 cells/sample. After seeding the cells, all samples were incubated at 37 °C in 5 % CO_2 for 1 and 7 days. Afterwards, the WST-8 cell counting kit was used to examine the cell viability. After 1 and 7 days of culturing, the cells were incubated with 5 % (v/v) WST-8 in the cell medium for 3 h. Then, the absorbance was measured at a wavelength of 450 nm using a microplate reader.

For comparison, the cytotoxicity of the various concentrations of tea polyphenols was performed using an indirect cell viability assay. In this regard, NHDF cells were seeded into a 24-well plate separately at a density of 10^5 cells/well and incubated at 37 °C in 5 % CO_2 for 24 h. In the next step, to prepare the extract medium sample, tea polyphenols (consisting of 5 mg/ml, 0.5 mg/ml, and 0.05 mg/ml) were submerged in the cell medium 24 h at 37 °C. Afterward, the cells were incubated with these extracted solutions for another 48 h. After 48 h of incubation, the cells were treated with 1 % (v/v) WST-8 diluted in the related cell medium. Finally, the absorbance was measured after 3 h of incubation at 450 nm by a microplate reader.

3. Results

3.1. Surface topography and chemical composition (SEM-EDS, FTIR-ATR)

Surface topography (SEM images at low and high magnifications, 100 – 1000×) and semi-quantitative chemical compositions (at% of elements from EDS analyses) are shown in Fig. 1 (AZ31, AZ31-pol, and AZ31-TPH30) and in Fig. 2 (AZ91, AZ91-blast, and AZ91-TPH30).

As-received AZ31 samples (Fig. 1 – AZ31) had an irregular surface (scratches and white oxide spots) deriving from mechanical processing and uncontrolled surface oxidation, as confirmed by EDS analyses, which evidenced a significant amount of oxygen.

After polishing (Fig. 1 – AZ31-pol), the surface was more regular (only thin polishing tracks were visible at 1000x magnification) and less oxidized. The surface oxygen content was reduced by almost an order of magnitude, while magnesium was almost doubled.

The polyphenol coating (Fig. 1 – AZ31-TPH30) was a homogeneous layer of microspheres uniformly distributed on the surface, without notable defects (no cracks or uncoated areas). The significant increase in the surface carbon content confirmed the organic nature of this layer.

As-cast AZ91 samples (Fig. 2 – AZ91) showed the typical grooved pattern reflecting the shape of the 3D-printed model with an irregular surface texture (typical layered texture originating from the 3D-printing

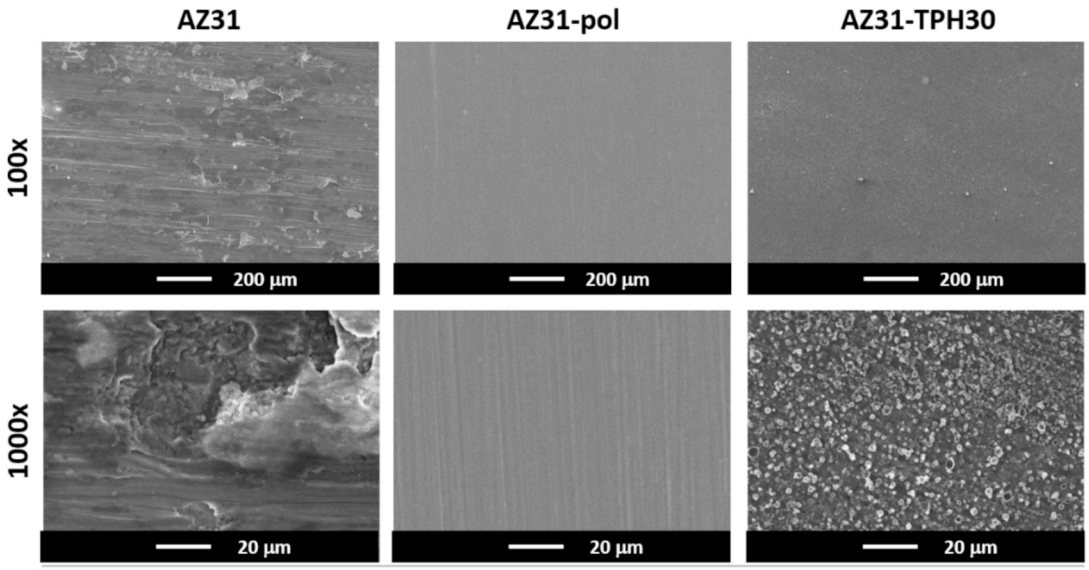

%at	AZ31	AZ31-pol	AZ31-TPH30
C	5.38±4.13	7.27±2.67	26.88±0.93
O	35.04±1.86	3.23±1.67	28.05±2.97
Mg	57.77±5.71	87.00±4.50	43.76±3.57
Al	1.73±0.29	2.35±0.06	1.32±0.34
Si	0.08±0.009	0.16±0.22	-

Fig. 1. SEM images and EDS analyses of AZ31 samples as-received (AZ31), polished (AZ31-pol), and coated with tea polyphenols (AZ31-TPH30).

process). Numerous deposits (clear globules in the 1000x image) were observed at higher magnification, which can be identified, by EDS analyses, as residuals from the ceramic mold.

After blasting (Fig. 2 – AZ91-blast), plaster remnants were removed, as confirmed by SEM images (no more clear globules visible in the 1000x image) and EDS analyses. The topography was the typical rough one of blasted surfaces.

As previously observed for AZ31 samples, polyphenol coating (Fig. 2 – AZ91-TPH30) appeared as a homogeneous layer of microspheres uniformly distributed on the surface following the substrate characteristic topography without notable defects (no cracks or uncoated areas). The significant increase in the surface carbon content confirmed, also in this case, the organic nature of this layer.

SEM images of AZ31 as received, washed, and coated with different concentrations of TPH are shown in the Supplementary material (Fig. S1), while SEM images of as-cast AZ91 washed and coated with TPH30 are reported in Fig. S2 of the Supplementary material.

Fig. S1 highlight that the coating of as-received AZ31 (without polishing) results in a non-homogeneous surface, documented by spotted surfaces with only partial coverage. Moreover, the use of diluted solutions (Fig. S1– AZ31 TPH5) evidences numerous micrometric cracks.

Similarly, the coating on as-cast AZ91 (without blasting – Fig. S2) resulted in the proper globular morphology, but was limited to certain areas of the surface (not homogeneous) and also full of cracks.

In summary, surface coating of as received/as cast surfaces resulted in non-homogeneous covering, as well as the use of more diluted TPH solutions. In particular, lower TPH concentration or longer soaking time resulted in non-homogeneous coatings, with the formation of a cracked reaction layer on the surface. On the contrary, coatings obtained in an orbital shaker with a TPH concentration of 30 mg/ml and a soaking time of 10 min (Figs. 1 and 2) were homogeneous and free of cracks on polished AZ31 and blasted AZ91. These can be considered as the optimized conditions of the process, as described in detail above.

The FTIR-ATR spectrum of the extract of tea polyphenols (TPH) shows a broad band centered around 3300 cm^{-1} attributable to OH groups, two signals at 2900 and 2840 cm^{-1} attributable to CH and OH functionalities in alkane and carboxylic acids, a signal at 1690 cm^{-1} related to C═O, a signal at 1612 cm^{-1} ascribable to C=C in the aromatic ring, a signal around 1500 cm^{-1} attributable to the stretching in the aromatic ring, a signal around 1450 cm^{-1} associated with C–H, two signals at 1360 and 1230 cm^{-1} related to phenolic OH, and a signal at 1030 cm^{-1} attributable to C–O–C [32,33].

These signals are consistent with the presence of epicatechin, epigallocatechin, epicatechin gallate, and epigallocatechin gallate, as main constituents of green tea polyphenols [34].

The molecular structure of the main components of green tea polyphenols cited above is shown in Fig. 4.

As expected, the spectra of AZ31 and AZ91 samples do not show any significant signal.

On the contrary, FTIR-ATR spectra of tea polyphenol-coated Mg alloys (AZ31-TPH30 and AZ91-TPH30) have a series of clear signals close to those of TPH extract, supporting the successful coating already evidenced by SEM-EDS. Some differences can be highlighted, as a shift of the signal at 1690 cm^{-1} (C=O) to 1598 cm^{-1} and of the signal at 1612 cm^{-1} (C=C) to 1500 cm^{-1} due to the formation of polyphenol-metal complexes mediated by carboxylic groups, as suggested in [35]. The interaction between carboxylic groups and the metal is also supported by the reduction of the signal at 2848 cm^{-1} observable on the coated Mg alloys. Moreover, a signal around 700 cm^{-1} can be observed on AZ31-TPH30 and AZ91-TPH30, which can be associated with the interaction between polyphenols and metal [35–37].

Through this analysis, we confirmed the effective presence of the TPH coating and that it had a chemical interaction with the metal substrate.

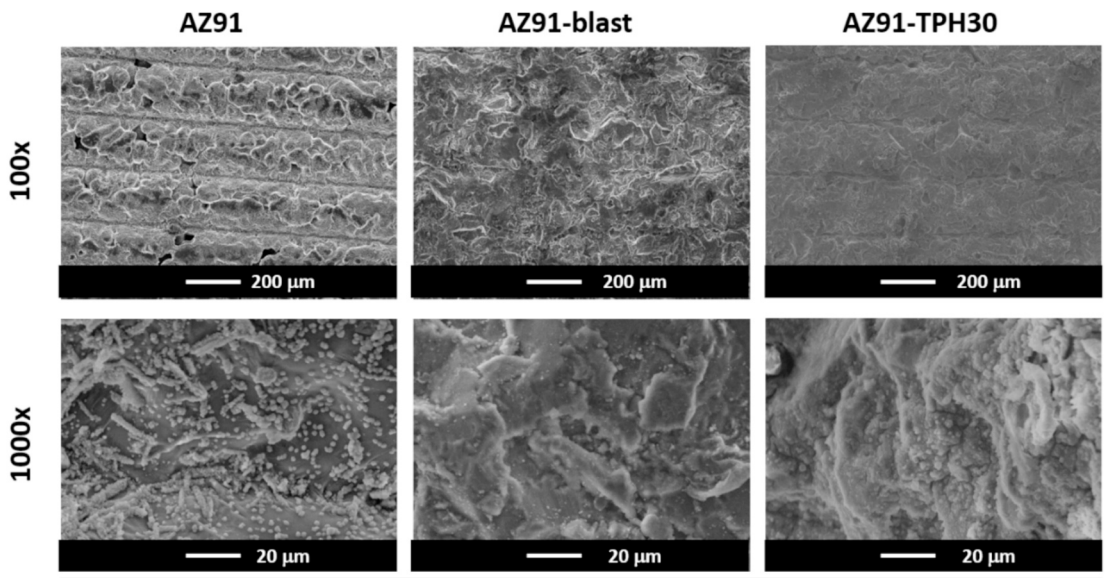

%at	AZ91	AZ91-blast	AZ91-TPH30
C	8.95±3.05	8.19±2.05	27.65±0.97
O	44.49±4.61	43.25±1.89	41.89±1.73
Mg	30.10±4.28	44.58±0.95	27.35±1.66
Al	4.03±0.25	3.98±0.67	3.10±0.98
Si	2.95±0.91		
S	2.89±0.75		
Ca	6.59±0.75		

Fig. 2. SEM images and EDS analyses of AZ91 samples as-casted (AZ91), blasted (AZ91-blast), and coated with tea polyphenols (AZ91-TPH30).

3.2. Coating adhesion (Tape test)

The adhesion of the polyphenolic coating to the magnesium substrates was evaluated by means of the tape test according to the ASTM D3359 standard.

Fig. 5 shows the appearance of the samples before and after the test, the tape after the test (a) and higher magnification SEM images of the surfaces after the test (b).

Looking at Fig. 5, it is evident that the coating only slightly detached during the test (further estimated as less than 5 %). In fact, the sample maintained the typical brownish color. Only a weak halo was present on the tape, suggesting a good adhesion of tea polyphenol coating on both AZ31 and AZ91 alloys. The results were confirmed by SEM images (Fig. 5b), where microspheres, characteristic of the coating, were still visible out of the cutter incisions after the tape removal.

3.3. Static degradation of the samples soaked in PBS

For the degradation tests, each coated alloy was compared with its control (the substrate used for the coating): the polished substrate for AZ31 and the blasted substrate for AZ91.

pH measurements are shown in Table 3.

The starting pH of PBS solution was 7.50, while it rose to 7.75 at 24 h of soaking of AZ31-pol and progressively increased up to 9.08 at 7 d. A similar behavior was observed for AZ31-TPH30, recording a pH of 7.77 at 24 h, which progressively rose to 9.50 in 7 days of soaking.

As far as AZ91 alloy is concerned, a rapid rise to pH 11.5 was observed at 24 h for both AZ91-blast and AZ91-TPH30 and remained almost constant up to 7 days for both samples.

Even if AZ31 is always reported as more reactive than AZ91, the polished alloy was able to maintain the pH almost at physiological values up to 24 h. On the contrary, blasted AZ91 showed a rapid pH rise in the first 24 h.

Despite the homogeneous surface coverage, the absence of cracks, and the good adhesion, TPH coatings were not able to control pH rise in PBS, even at short times, on both alloys, showing a behavior close to the substrates. An explanation of these results will be presented in the discussion section.

The Mg release in the PBS soaking solution evidenced average values of 7.5 mg/ml for AZ31-pol and 9 mg/ml for AZ31-TPH30 at 24 h, rising up to 14 mg/ml for AZ31-pol and 29 mg/ml for AZ31-TPH30 at 7 days.

AZ91-blast released 13 mg/ml of Mg at 24 h compared to 8 mg/ml of AZ91-TPH30, but both samples stabilized their release at 150 mg/ml at 7 days.

The values of Mg-release were in accordance with the pH ones, evidencing the rate of degradation of the alloys in PBS.

The Folin&Ciocalteu test evidenced a release of polyphenols of around 0.03–0.04 mg/ml (GAE Gallic Acid equivalents) for coated samples during the degradation test in PBS.

3.4. Electrochemical corrosion tests

Fig. 6a shows Tafel curves, in a range of test media, simulating physiological solutions of different complexity, of uncoated and TPH30-

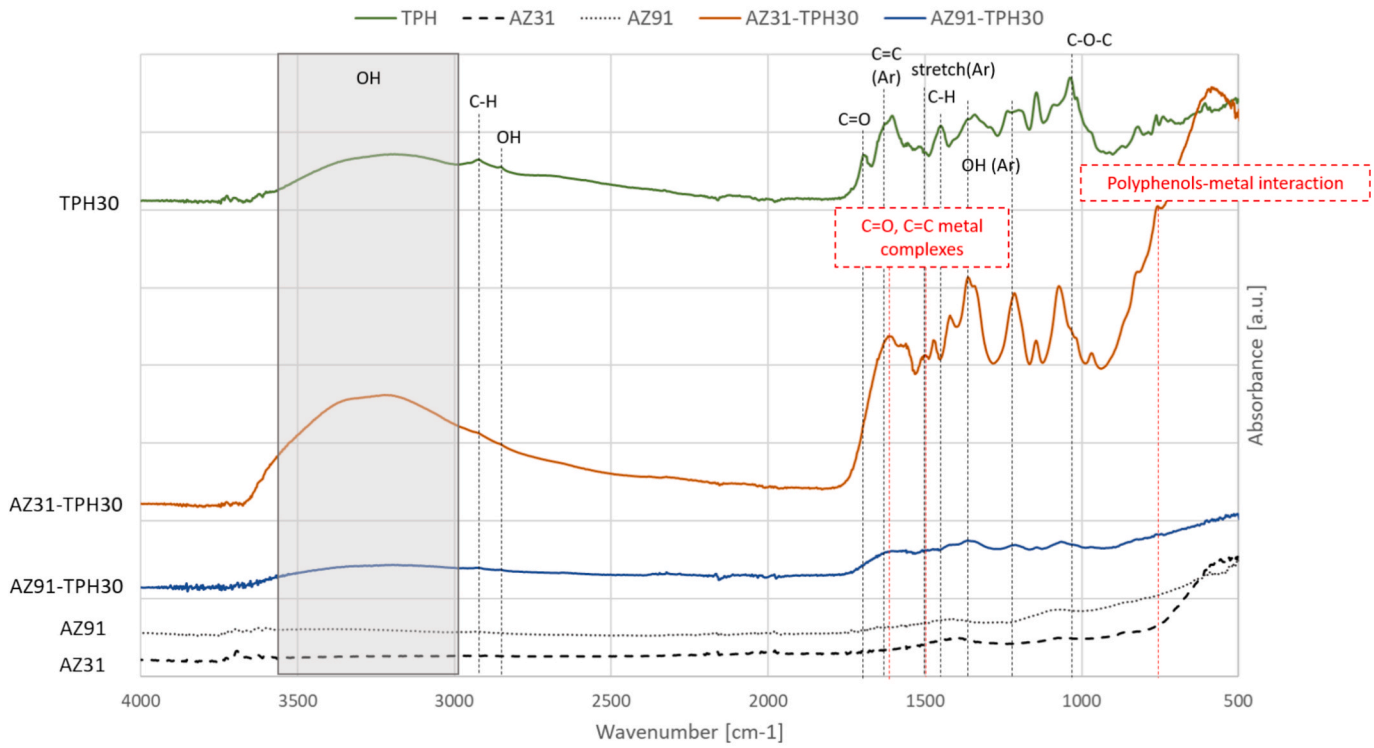

Fig. 3. FTIR-ATR spectra of TPH, AZ31, AZ91, AZ31-TPH30, and AZ91-TPH30 samples.

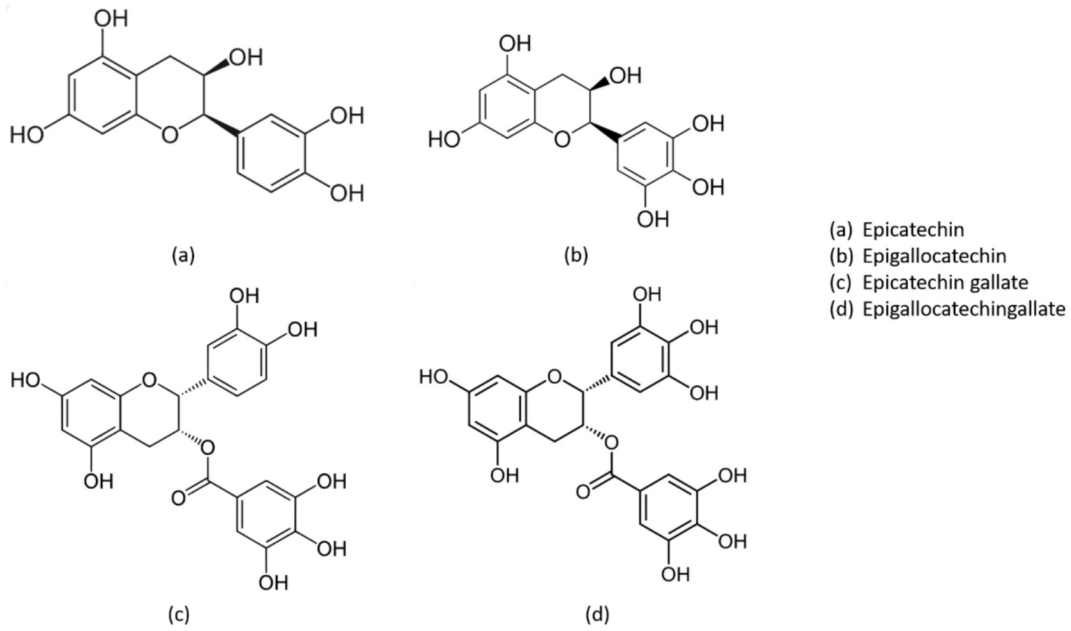

Fig. 4. Molecular structure of the main constituents of tea polyphenols.

coated AZ31 specimens. Fig. 6b shows the corresponding curves for AZ91 specimens. Representative data were chosen as the most reproducible and clear during several measurements. A higher level of variability was observed on AZ31 specimens in comparison with AZ91, which exhibited more symmetrical and reproducible polarization behavior.

A first comparison was made by considering the E_{corr}. For AZ31, a significant anodic shift of E_{corr} for coated specimens in HBSS, HBSS2, and PBS revealed the presence of a passivation protecting layer. Coated AZ31 specimens (AZ31-TPH30) in DMEM and Ringer's fluid, however, had a cathodic shift, which implied poor corrosion inhibition in these liquids. The range of E_{corr} values for AZ31 samples varies from – 1.67 V to–1.38 V.

Unlike AZ31, AZ91 samples revealed a relatively narrow range of E_{corr} (–1.50 V to–1.45 V), with comparable values for coated and uncoated groups. This indicated a more consistent electrochemical

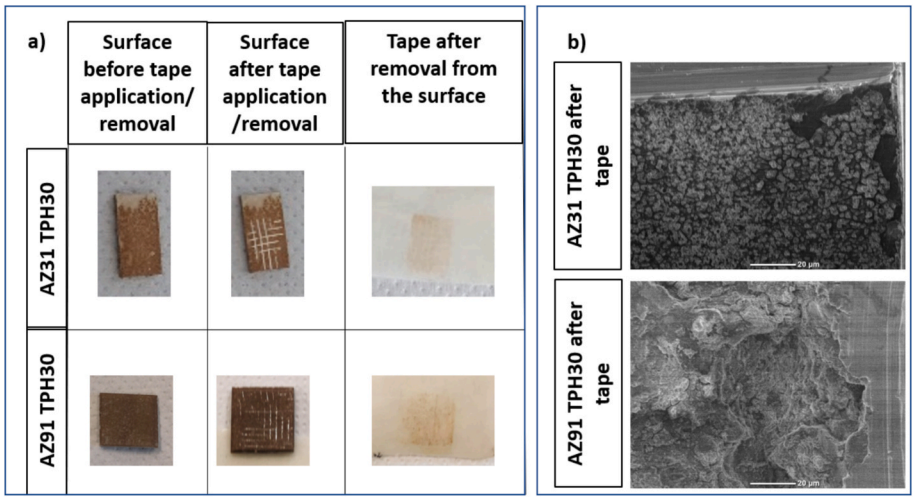

Fig. 5. Tape adhesion test on AZ31-TPH30 and AZ91-TPH30: a) Macro-images of the coated surfaces before and after the test and the tape after the test, b) SEM images of the surfaces after the tape.

Table 3
Ph measurements in the static degradation test.

Sample	pH			
	0 h	24 h	48 h	7d
AZ31-pol	7.50	7.75	7.82	9.08
AZ31-TPH30	7.50	7.77	7.74	9.50
AZ91-blast	7.50	11.60	11.10	11.40
AZ91-TPH30	7.50	11.50	11.20	11.30

behavior. Nevertheless, AZ91-TPH30-coated samples systematically exhibited a higher corrosion activity.

A further comparison was made by considering the corrosion rate. Corrosion rate results of AZ31 alloy are shown in Fig. 7a and those of AZ91 in Fig. 7b. In all test solutions, TPH30-coated specimens had low corrosion rate values compared to controls, which also validated suppressed electrochemical reactivity and enhanced corrosion protection.

Polished AZ31 samples demonstrated inherently lower corrosion rates than sandblasted AZ91, attributed to smoother surface morphology. For AZ91, the ratio between the corrosion rate of uncoated AZ91 and coated AZ91 (AZ91-TPH) is approximately 1.5/2 in the tested fluids, indicating a significant improvement in corrosion resistance (corrosion rate is approximately reduced by half in coated samples).

AZ31, despite being more variable, shows even more substantial improvements; in fact, even if the ratio between the uncoated and coated alloy remained similar to that obtained for AZ91 in HBSS2 and DMEM, in PBS and Ringer infusions, the ratio is 3 (the corrosion rate reduced by approximately 1/3 in coated samples), and in HBSS, it is 8.5 (corrosion rate reduced by 1/9). This makes the TPH30 coating even more functional for this alloy when in contact with these fluids.

The corrosion parameters (E_{corr}, i_{corr} and corrosion rate) obtained from the polarization curves for all conditions are presented separately in Fig. 8.

3.5. Biological characterization

Fig. 9 shows the cell viability after 1 and 7 days of incubation with different samples: polyester control (CTL), uncoated magnesium alloys (AZ31-pol and AZ91-blast), and the same alloys coated with polyphenols (AZ31-TPH30 and AZ91-TPH30).

At day 1, AZ91 exhibited higher cell viability than AZ31, likely due to the initial promotion of fibroblast adhesion. However, a significant decrease in cell viability occurred at day 7. This can be explained by considering that the rapid corrosion of AZ91 led to cytotoxic effects. In contrast, AZ31 showed a lower adhesion than AZ91 at day 1, but a lower decrease in viability over time, consistent with its slower degradation rate, observed in the PBS degradation test and electrochemical corrosion

The application of the TPH30 polyphenol coating appeared to slightly mitigate cytotoxicity at day 1 in both alloys by reducing ion release and corrosion. The cell viability was increased on AZ91-TPH vs AZ91 and the variability in vitality was reduced on AZ31-TPH30 vs AZ31. Nonetheless, the protective effect diminished at day 7, especially on AZ91, where corrosion progressed and negatively impacted cell viability, in accordance with static degradation tests in PBS. AZ31-TPH30 showed the highest cell vitality at 7 days among the tested Mg samples, even if it was low.

A trend with about double cell viability on coated Mg-alloys compared to the uncoated ones has been reported in the literature for catechin-coated Mg [21]. Moreover, cell viability is always reported as lower than traditional non-biodegradable metals (e.g. stainless steel) and strongly dependent on test conditions.

Indirect tests on the polyphenol extract evidenced a cytotoxicity limit close to 0.5 mg/ml.

Comparing these results with the polyphenols release in PBS (0.03–0.04 mg/ml), it is clear that eventual toxicity is not induced by the presence of biomolecules, as discussed above.

4. Discussion

As reported in the literature [38], the surface preparation significantly affects the reactivity and corrosion of Mg alloys, affecting the presence of irregularities and contaminants. This pre-treatment is also expected to strongly affect the deposition of the coating of biomolecules: this is why several surface conditions were explored for the coating with an extract of green tea polyphenols. Some of the authors previously investigated the effect of surface pre-treatments on the ability of the steel to effectively bind tannins [39]. However, pre-treatments of magnesium alloys for protective coating deposition are still poorly discussed in the literature. These treatments play a crucial role in coating formation, especially when there is a chemical interaction between coating molecules (polyphenols) and metal ions/atoms on the substrates, or released by them, during the coating formation.

Continuous and almost free of cracks coatings were obtained on polished AZ31 and blasted AZ91, as shown in Figs. 1 and 2. On the other hand, non-homogeneous, thin and discontinuous coatings were obtained on as-received AZ31 and as-cast AZ91 surfaces, as shown in Supplementary materials. These results can be explained considering that polishing and blasting remove contaminations and make the surface

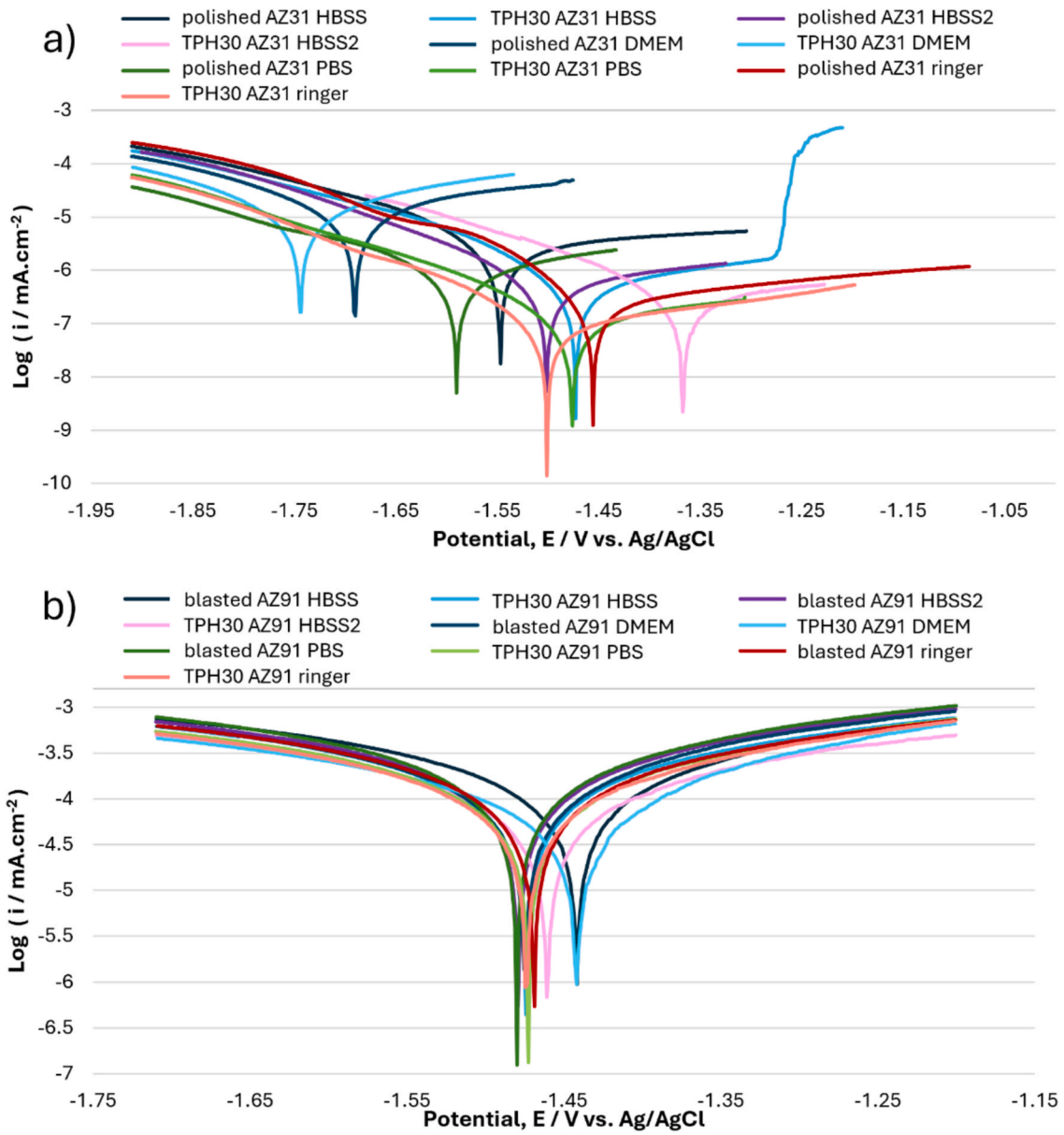

Fig. 6. a) Tafel curves of TPH30-coated and uncoated (control) AZ31 samples tested in different fluids. b) Tafel curves of TPH30-coated and uncoated (control) AZ91 samples tested in different fluids.

more homogeneous (Figs. 1 and 2) and reactive toward the polyphenolic solution.

Polishing of AZ31 alloy also contributes to its corrosion resistance. The as-received AZ31 alloy [24] showed a rapid pH rise up to 10 in 1 day, maintained until 3 days, and followed by a moderate decrease only at 7 and 8 days. On the contrary, the polished AZ31 samples had a small pH rise from 7.5 to 7.7 at 1 day. It progressively increased up to 9 at 7 days.

The necessity to expose a clean and reactive Mg-surface to the polyphenolic solution for obtaining an effective coating is also supported by FTIR results (Fig. 3), which highlighted the formation of Mg-polyphenol complexes. Proper balancing of surface reactivity, Mg^{2+} ion release, and polyphenol deposition allows effective coating, as explained in the following.

The formation of catechin-based coatings as a compact layer of polyphenol-Mg spheres was obtained by the addition of Mg^{2+} ions into the polyphenolic solution and the application of a layer-by-layer procedure, as reported in the literature [21]. In the present research, we can suppose a similar mechanism where Mg^{2+} ions were made available in the polyphenolic solution by direct release from the substrates. The formation of microspheres is a typical morphology of catechins on magnesium surfaces and cannot be ascribed to bubble formation during coating. A proper balance between surface preparation, soaking time, and solution concentration was optimized in order to obtain a compact layer of spheres in a single passage.

Considering these results, it can be supposed that the mechanism of coating formation is based on the complexation of tea polyphenols with Mg^{2+} ions, released from the substrate during soaking, and the grafting of the complexes to surface OH groups. The hypothesis is supported by FTIR-ATR spectra discussed above.

The obtained coating is well adhered to the substrate, as demonstrated by the tape test.

The coating is thin, but it is difficult to make a precise measurement of thickness due to its small size and globular structure. The roughness of the substrate makes the measurement further complex. However, considering that magnesium and aluminum were still visible in EDS analyses and that FTIR-ATR clearly detected the coating, we can suppose a coating thickness in the micron range, probably not exceeding 1 μm,

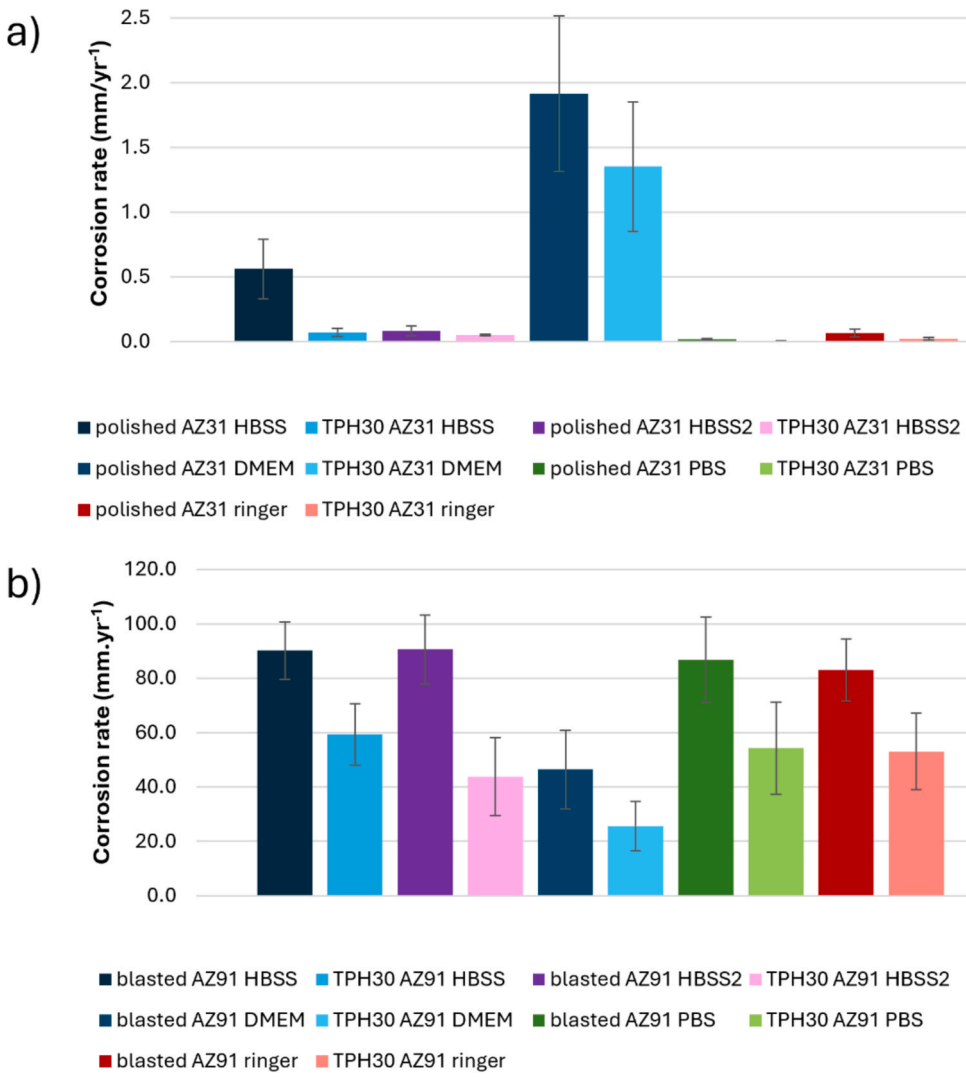

Fig. 7. a) Histogram comparing the corrosion rate of AZ31 samples tested in different fluids. b) Histogram comparing the corrosion rate of AZ91 samples tested in different fluids.

since the penetration depth of both EDS and FTIR-ATR is in the micron range.

However, coating performances in static degradation tests in PBS were not good for both AZ31-TPH30 and AZ91-TPH30. The cause of degradation during soaking cannot be ascribed to the generalized presence of cracks on these coatings, as it was for the tannic acid ones previously obtained by the authors [24], considering that the coatings described in this paper were almost free of cracks. On the contrary, these coatings showed a significant protection ability in electrochemical corrosion tests.

These results suggest a pronounced effect of local cracks on the static degradation tests in PBS, compared to the electrochemical resistance of the samples. It must be considered that only a central portion of the surface is exposed to the electrolyte, while the whole sample (with possible localized edge defects) is immersed in the solution in static degradation tests.

The consistent reduction in corrosion rates in both AZ31 and AZ91 coated samples across different testing media is attributed to the strong ability of the TPH30 coating to mitigate electrochemical degradation.

Although all coated samples exhibited greater corrosion resistance compared to the uncoated ones, AZ31 samples generally showed a higher resistance to corrosion. This may be attributed to their lower aluminum content compared to AZ91 [40], as well as the use of surface polishing instead of sandblasting [41], as was done for AZ91.

The improved corrosion resistance of coated AZ31 and AZ91 is attributed to the formation of a uniform coating with minimal cracks. This coating adheres well to the substrate, limiting electrolyte penetration and suppressing the localized corrosion.

All samples were examined in a range of fluids to assess the impact of a range of ions and organic species on the corrosion of coated and uncoated AZ91 and AZ31 alloys. In the case of AZ31, DMEM proved most corrosive under electrochemical conditions, whilst HBSS was the most corrosive for AZ91 samples. This difference in corrosion behavior could be due to variations in surface morphology for AZ31 and AZ91, a lower content of aluminum for AZ31, and the differing ionic compositions of the test media, which can work in a complex manner on the exposed surfaces.

Altogether, the soaking and electrochemical results underline that the corrosion of magnesium alloys is strongly dependent on the testing condition. The problem is known and discussed in the scientific literature [42], but not completely understood and solved. In particular, for biomedical applications, the difficulty in mimicking physiological conditions makes this issue more critical for proper material development and characterization.

The same consideration can be applied to biological tests. It is not easy to set an in vitro evaluation of Mg-based alloys due to their strong

HBSS	i_{corr} (A.cm^{-2})	E_{corr} (V)	Corrosion rate (mm.yr^{-1})
polished AZ31	3.63E-05	-1.509	0.563±0.230
TPH30 AZ31	3.21E-06	-1.472	0.072±0.030

HBSS	i_{corr} (A.cm^{-2})	E_{corr} (V)	Corrosion rate (mm.yr^{-1})
blasted AZ91	0.0042	-1.463	90.2±10.5
TPH30 AZ91	0.0029	-1.477	59.3±11.4

HBSS2	i_{corr} (A.cm^{-2})	E_{corr} (V)	Corrosion rate (mm.yr^{-1})
polished AZ31	2.22E-06	-1.480	0.084±0.038
TPH30 AZ31	2.31E-06	-1.446	0.052±0.007

HBSS2	i_{corr} (A.cm^{-2})	E_{corr} (V)	Corrosion rate (mm.yr^{-1})
blasted AZ91	0.0044	-1.488	90.6±12.6
TPH30 AZ91	0.0027	-1.466	43.8±14.4

DMEM	i_{corr} (A.cm^{-2})	E_{corr} (V)	Corrosion rate (mm.yr^{-1})
polished AZ31	7.60E-05	-1.605	1.915±0.581
TPH30 AZ31	1.79E-04	-1.678	1.352±0.487

DMEM	i_{corr} (A.cm^{-2})	E_{corr} (V)	Corrosion rate (mm.yr^{-1})
blasted AZ91	0.0022	-1.481	46.4±14.5
TPH30 AZ91	0.0012	-1.479	25.7±9

Ringer infusions	i_{corr} (A.cm^{-2})	E_{corr} (V)	Corrosion rate (mm.yr^{-1})
polished AZ31	8.56E-07	-1.383	0.019±0.005
TPH30 AZ31	4.77E-07	-1.435	0.006±0.002

Ringer infusions	i_{corr} (A.cm^{-2})	E_{corr} (V)	Corrosion rate (mm.yr^{-1})
blasted AZ91	0.0047	-1.478	86.8±15.7
TPH30 AZ91	0.0042	-1.497	54.3±17.0

PBS	i_{corr} (A.cm^{-2})	E_{corr} (V)	Corrosion rate (mm.yr^{-1})
polished AZ31	2.90E-06	-1.544	0.067±0.028
TPH30 AZ31	3.13E-05	-1.496	0.021±0.010

PBS	i_{corr} (A.cm^{-2})	E_{corr} (V)	Corrosion rate (mm.yr^{-1})
blasted AZ91	0.0039	-1.486	82.9±11.4
TPH30 AZ91	0.0034	-1.484	53.1±14.0

Fig. 8. Corrosion parameters of all samples in HBSS, HBSS2, DMEM, Ringer solution, and PBS.

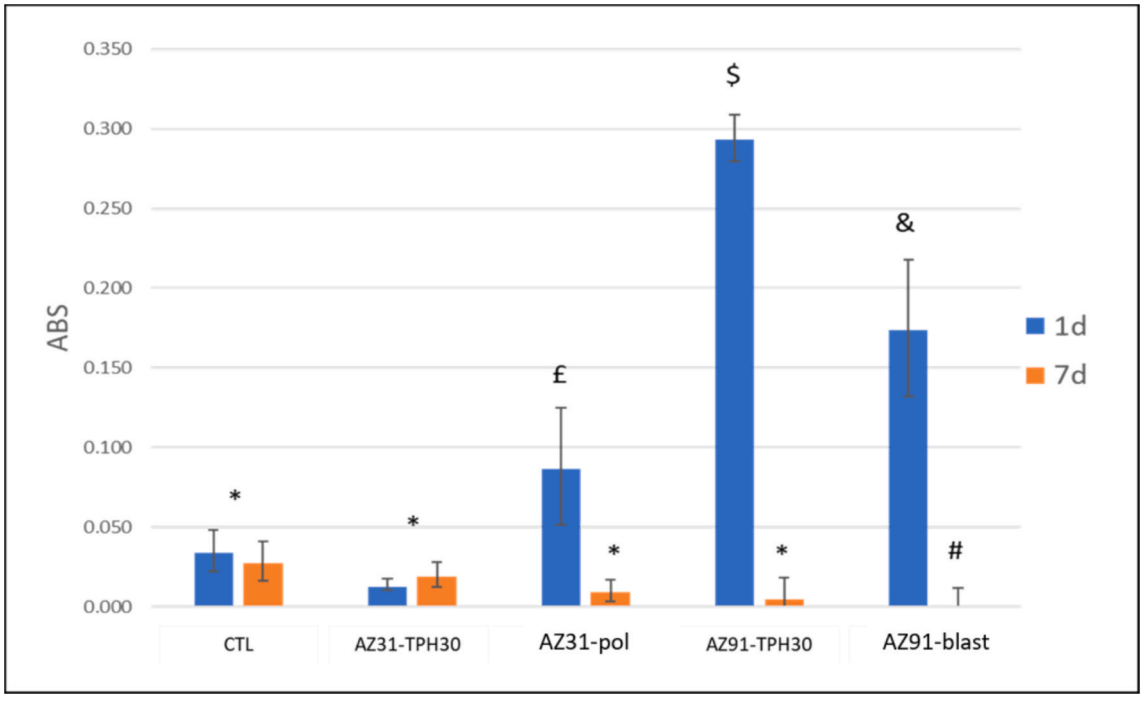

Fig. 9. Cell viability in absorbance (ABS) after 1 and 7 days of incubation with different samples: polyester control (CTL), magnesium alloys AZ31-pol and AZ91-blast, and the same alloys coated with polyphenols (AZ31-TPH30 and AZ91-TPH30).

reaction in contact with cells. In a static environment, the direct contact of cells with a substrate which rapidly reacts, developing gases and degradation products, which are not removed by the culture medium, makes the simulation of a physiological environment complex and not completely controllable. Monitoring the effects on the cell response of the testing medium composition and eventual flow, as a function of time and setup of the test, is crucial for a significant model [43–45].

In the present research, preliminary biological experiments clearly highlighted the complexity of direct in vitro cell cultures, but also showed the potentialities of polyphenol coating on the modulation of

the biological response of magnesium alloys. In fact, tea polyphenols did not result in toxicity at the concentrations released from the coated alloys. Moreover, TPH-coated alloys protected cells, despite a still rapid degradation and consequent adverse effects associated with a static direct approach previously discussed.

Future optimization of in vitro testing models will open new opportunities in the investigation of sustainable organic coatings able to modulate the degradation of Mg-based alloys for biomedical applications and their biological response.

5. Conclusion

Green Tea Polyphenols (TPH) have been successfully used to obtain a crack-free globular coating on AZ-31 and AZ91 Mg alloys. Surface pretreatments resulted to be crucial for a continuous and well-adhered coating based on the direct interaction of polyphenols with magnesium. TPH coatings reduced the corrosion rate in electrochemical tests and promoted cellular protection from the rapid magnesium degradation, in preliminary in vitro tests.

Results suggested tea polyphenols to be promising for protective layers to control the degradation rate of magnesium alloys, as well as proper in vitro tests and degradation models are needed to monitor and investigate the magnesium alloys in simulated physiological conditions.

CRediT authorship contribution statement

S. Ferraris: Writing – review & editing, Writing – original draft, Supervision, Methodology, Investigation, Data curation, Conceptualization. **S. Spriano:** Writing – review & editing, Writing – original draft, Supervision, Resources, Methodology, Conceptualization. **F. Gamna:** Writing – review & editing, Writing – original draft, Visualization, Investigation. **M. Saqib:** Writing – review & editing, Writing – original draft, Methodology, Investigation. **N. Beshchasna:** Writing – review & editing, Writing – original draft, Supervision, Methodology. **J. Opitz:** Writing – review & editing, Writing – original draft, Supervision, Resources. **A.R. Boccaccini:** Writing – review & editing, Writing – original draft, Supervision, Resources, Methodology. **Irem Unalan:** Writing – review & editing, Writing – original draft, Visualization, Investigation. **K. Naplocha:** Writing – review & editing, Writing – original draft, Supervision, Resources, Methodology, Conceptualization. **A. Dmitruk:** Writing – review & editing, Writing – original draft, Supervision, Methodology, Investigation, Conceptualization.

Declaration of competing interest

The authors declare that they have no known competing financial interests or personal relationships that could have appeared to influence the work reported in this paper.

Acknowledgment

Part of this work was supported by the European Virtual Institute on Knowledge-based Multifunctional Materials AISBL (KMM-VIN) in the frame of the KMM-VIN Research Fellowship program (15th call, 2023).

Appendix A. Supplementary data

Supplementary data to this article can be found online at https://doi.org/10.1016/j.apsusc.2025.165402.

Data availability

Data will be made available on request.

References

[1] V. Tsakiris, C. Tardei, F.M. Clicinschi, Biodegradable Mg alloys for orthopedic implants –a review, J. Magnes. Alloys 9 (2021) 1884–1905.
[2] Y. Yang, C. He, W. Yang, F. Qi, D. Xie, L. Shen, S. Peng, C. Shuai, Mg bone implant: Features, developments and perspectives, Mater. Des. 185 (2020) 108259.
[3] S. Wang, C. Du, X. Shen, X. Wu, S. Ouyanga, J. Tan, J. She, A. Tang, X. Chen, F. Pan, Rational design, synthesis and prospect of biodegradable magnesium alloy vascular stents, J. Magnes. Alloys 11 (2023) 3012–3037.
[4] F. Witte, The history of biodegradable magnesium implants: a review, Acta Biomater. 6 (2010) 1680–1692.
[5] J. Wang, J. Dou, Z. Wang, C. Hu, H. Yu, C. Chen, Research progress of biodegradable magnesium-based biomedical materials: a review, J. Alloy. Compd. 923 (2022) 166377.
[6] J. Kim, H. Pan, Effects of magnesium alloy corrosion on biological response – Perspectives of metal-cell interaction, Prog. Mater Sci. 133 (2023) 101039.
[7] D.W.Y. Toong, J.C.K. Ng, Y. Huang, P.E.H. Wong, H.L. Leo, S.S. Venkatraman, H. Y. Ang, Bioresorbable metals in cardiovascular stents: material insights and progress, Materialia 12 (2020) 100727.
[8] J. Dong, T. Lin, H. Shao, H. Wang, X. Wang, K. Song, Q. Li, Advances in degradation behavior of biomedical magnesium alloys: a review, J. Alloy. Compd. 908 (2022) 164600.
[9] Z.-Q. Zhang, Y.-X. Yang, J.-A. Li, R.-C. Zeng, S.-K. Guan, Advances in coatings on magnesium alloys for cardiovascular stents – a review, Bioact. Mater. 6 (2021) 4729–4757.
[10] M. Echeverry-Rendon, J.P. Allain, S.M. Robledo, F. Echeverria, M.C. Harmsen, Coatings for biodegradable magnesium-based supports for therapy of vascular disease: a general view, Mat Sci Eng C 102 (2019) 150–163.
[11] D. Zhang, F. Peng, X. Liu, Protection of magnesium alloys: from physical barrier coating to smart self-healing coating, J. Alloy. Compd. 853 (2021) 157010.
[12] G. Wu, J.M. Ibrahim, P.K. Chu, Surface design of biodegradable magnesium alloys — a review, Surf Coat Tech 233 (2013) 2–12.
[13] J. Singh, A.W. Hashmi, S. Ahmad, Y. Tian, Critical review on biodegradable and biocompatibility magnesium alloys: progress and prospects in bio-implant applications, Inorg. Chem. Commun. 169 (2024) 113111, https://doi.org/10.1016/j.inoche.2024.113111.
[14] Z. Xue, X. Sun, H. Li, M. Iqbal, L. Qi, F. Wang, Y. Hou, J. Li, S. Guan, Composite coatings of S-HA nanoparticles and Schiff base on ZE21B alloy for stronger corrosion resistance and biological performance, JMA 12 (2024) 4547–4560, https://doi.org/10.1016/j.jma.2023.11.009.
[15] M. Kaseem, Y.G. Ko, Morphological modification and corrosion response of MgO and Mg3(PO4)2 composite formed on magnesium alloy, Compos. B Eng. 176 (2019) 107225, https://doi.org/10.1016/j.compositesb.2019.107225.
[16] A. Keyvani, N. Kamkar, R. Chaharmahali, M. Bahamirian, Mosab Kaseem, Arash Fattah-alhosseini, Improving anti-corrosion properties AZ31 Mg alloy corrosion behavior in a simulated body fluid using plasma electrolytic oxidation coating containing hydroxyapatite nanoparticles, Inorg. Chem. Commun. (Part 1) (2023), https://doi.org/10.1016/j.inoche.2023.111470.
[17] M.A. Khan, A.R. Safira, M. Aadil, M. Kaseem, Development of anti-corrosive coating on AZ31 Mg alloy modified by MOF/LDH/PEO hybrids, JMA 12 (2024) 586–607, https://doi.org/10.1016/j.jma.2023.12.004.
[18] A.S. Gnedenkov, S.L. Sinebryukhov, V.S. Marchenko, A.D. Nomerovskii, A. Y. Ustinov, A. Fattah-alhosseini, S.V. Gnedenkov, Efficient and smart hybrid coatings for active corrosion protection of magnesium alloys, JMA 13 (2025) 4475–4499, https://doi.org/10.1016/j.jma.2025.07.017.
[19] S. Chen, S. Zhao, M. Chen, X. Zhang, J. Zhang, X. Li, H. Zhang, X. Shen, J. Wang, N. Huang, The anticorrosion mechanism of phenolic conversion coating applied on magnesium implants, Appl. Surf. Sci. 463 (2019) 953–967.
[20] H. Zhang, R. Luo, W. Li, J. Wang, M.F. Maitz, J. Wang, G. Wan, Y. Chen, H. Sun, C. Jiang, R. Shen, N. Huang, Epigallocatechin gallate (EGCG) induced chemical conversion coatings for corrosion protection of biomedical MgZnMn alloys, Corros. Sci. 94 (2015) 305–315.
[21] B. Zhang, R. Yao, L. Li, Y. Wang, R. Luo, L. Yang, Y. Wang, Green tea polyphenol induced Mg2+-rich multilayer conversion coating: toward enhanced corrosion resistance and promoted in situ endothelialization of AZ31 for potential cardiovascular applications, ACS Appl. Mater. Interfaces 11 (2019) 41165–41177.
[22] M. Asgari, Y. Yang, S. Yang, Z. Yu, P.K.D.V. Parlagadda, Y. Xiao, Z. Li, Mg−phenolic network strategy for enhancing corrosion resistance and osteocompatibility of degradable magnesium alloys, ACS Omega 4 (2019) 21931–21944.
[23] H. Zhang, B. Wang, J. Han, X. Shen, Q. Sun, Y. An, R. Luo, Y. Wang, A self-healing coating with embedding of polyphenols on magnesium: towards enhanced corrosion protection for biodegradable vascular implants, Chem. Eng. J. 482 (2024) 149020, https://doi.org/10.1016/j.cej.2024.149020.
[24] J. Barberi, M. Saqib, A. Dmitruk, J. Opitz, K. Naplocha, N. Beshchasna, S. Spriano, S. Ferraris, Characterization of tannic acid-coated AZ31 Mg alloy for biomedical application and comparison with AZ91, Materials 17 (2024) 343, https://doi.org/10.3390/ma17020343.
[25] S. Spriano, A. Dmitruk, K. Naplocha, S. Ferraris, Tannic acid coatings to control the degradation of AZ91 Mg alloy porous structures, Metals 13 (2023) 200, https://doi.org/10.3390/met13020200.
[26] M. Cazzola, I. Corazzari, E. Prenesti, E. Bertone, E. Vernè, S. Ferraris, Bioactive glass coupling with natural polyphenols: Surfacemodification, bioactivity and antioxidant ability, Appl. Surf. Sci. 367 (2016) 237–248.
[27] ASTM D 3359-97; Standard Test Methods for Measuring Adhesion by Tape Test. American Society for Testing and Materials: West Conshohocken, PA, USA, 1997.

[28] ASTM G31-72; Standard Practice for Laboratory Immersion Corrosion Testing of Metals. ASTM International: West Conshohocken, PA, USA, 1999.
[29] M. Saqib, O.S. Kuzmin, H. Kraskiewicz, L. Wasyluk, G. Cuniberti, A.A. Ficai, V. F. Pichugin, J. Opitz, N. Beshchasna, Evaluation of in vitro corrosion behavior of titanium oxynitride coated stainless steel stents, IEEE Access 9 (2021) 59766–59782.
[30] ASTM G102-89(2015)e1; Standard Practice for Calculation of Corrosion Rates and Related Information from Electrochemical Measurements. ASTM: West Conshohocken, PA, USA, 2023.
[31] I. Unalan, B. Slavik, A. Buettner, A.R. Boccaccini, Phytotherapeutic hierarchical PCL-based scaffolds as a multifunctional wound dressing: combining 3D printing and electrospinning, Macromol. Biosci. 24 (2024) 2400253.
[32] H. Wang, L. Chen, L.-L. Weng, M.-Y. Zhang, Q. Shen, Surface properties and dissolution kinetics of tea polyphenols, J. Adhes. Sci. Technol. 28 (2014) 2416–2423, https://doi.org/10.1080/01694243.2014.968420.
[33] M.A. Brza, S.B. Aziz, H. Anuar, F. Ali, E.M.A. Dannoun, S.J. Mohammed, R. T. Abdulwahid, S. Al-Zangana, Tea from the drinking to the synthesis of metal complexes and fabrication of PVA based polymer composites with controlled optical band gap, Sci. Rep. 10 (2020) 18108, https://doi.org/10.1038/s41598-020-75138-x.
[34] Y. Yang, T. Zhang, Antimicrobial activities of tea polyphenol on phytopathogens: a review, Molecules 24 (2019) 816, https://doi.org/10.3390/molecules24040816.
[35] I.I. Lungu, D. Marin-Batîr, A. Panainte, C. Mircea, C. Tuchiluş, A. Ştefanache, F. A. Szasz, D. Grigorie, S. Robu, O. Cioancă, M. Hăncianu, Catechin-zinc-complex: synthesis characterization and biological activity assessment, Farmacia 71 (2023) 755–763.
[36] S. Hamimed, N. Jebli, H. Sellami, A. Landoulsi, A. Chatti, Dual valorization of olive mill wastewater by bio-nanosynthesis of magnesium oxide and yarrowia lipolytica biomass production, Chem.Biodivers. 17 (2020) e1900608, https://doi.org/10.1002/cbdv.201900608.
[37] A. Zazoua, S. Bouraoui, N. Jaffrezic-Renault, Cu(II) adsorption onto a biopolymer extracted from a vegetable waste: application to a miniaturized electrochemical sensor, J. Inorg. Organomet. Polym. 28 (2018) 1914–1923, https://doi.org/10.1007/s10904-018-0874-z.
[38] U.C. Nwaogu, C. Blawert, N. Scharnagl, W. Dietzel, K.U. Kainer, Influence of inorganic acid pickling on the corrosion resistance of magnesium alloy AZ31 sheet, Corros. Sci. 51 (2009) 2544–2556.
[39] R. Sesia, S. SprianoM, M. Sangermano, S. Calovi, S.F. Rossi, Natural tannin layers for the corrosion protection of steel in contact with water-based media, Coatings 14 (2024) 965, https://doi.org/10.3390/coatings14080965.
[40] S.K. Woo, B.-C. Suh, H.S. Kim, C.D. Yim, Effect of Al addition on corrosion behavior of high-purity Mg in terms of processing history, J. Magnes. Alloys 11 (2023) 851–868, https://doi.org/10.1016/j.jma.2022.12.005.
[41] L. Kumar, A. Jain, K. Kumar, G.K. Sharma, Influence of surface polishing on the degradation behavior of biodegradable Magnesium alloy, Eng. Res. Express 5 (2020) 045032, https://doi.org/10.1088/2631-8695/ad04ac.
[42] D. Mei, S.V. Lamaka, X. Lu, M.L. Zheludkevich, Selecting medium for corrosion testing of bioabsorbable magnesium and other metals – a critical review, Corros. Sci. 171 (2020) 108722.
[43] O. Jung, D. Porchetta, M.L. Schroeder, M. Klein, N. Wegner, F. Walther, F. Feyerabend, M. Barbeck, A. Kopp, In vivo simulation of magnesium degradability using a new fluid dynamic bench testing approach, Int. J. Mol. Sci. 20 (2019) 4859, https://doi.org/10.3390/ijms20194859.
[44] F. Cecchinato, N.A. Agha, A.H. Martinez-Sanchez, B.J. Luthringer, F. Feyerabend, R. Jimbo, R. Willumeit-Römer, A. Wennerberg, Influence of magnesium alloy degradation on undifferentiated human cells, PLoS One 10 (2015) e0142117, https://doi.org/10.1371/journal.pone.0142117.
[45] J. Gonzalez, R.Q. Hou, E.P.S. Nidadavolu, R. Willumeit-Römer, F. Feyerabend, Magnesium degradation under physiological conditions – best practice, Bioact. Mater. 3 (2018) 174–185, https://doi.org/10.1016/j.bioactmat.2018.01.003.